Lawrence Berkeley National Laboratory
LBL Publications

Title
How the Hydrophobic Interface between a Perfluorosulfonic Acid Polymer and Water Vapor Controls Membrane Hydration

Permalink
https://escholarship.org/uc/item/9t3393kw

Journal
ACS Applied Polymer Materials, 4(5)

ISSN
2637-6105

Authors
Soniat, Marielle
Houle, Frances A

Publication Date
2022-05-13

DOI
10.1021/acsapm.1c01805

Peer reviewed

How the Hydrophobic Interface between a Perfluorosulfonic Acid Polymer and Water Vapor Controls Membrane Hydration

Marielle Soniat[#]* and Frances A. Houle*

Joint Center for Artificial Photosynthesis and Chemical Science Division, Lawrence Berkeley National Laboratory, Berkeley, CA 94720

* Corresponding authors: fahoule@lbl.gov, mesoniat2013@gmail.com

ABSTRACT

Stable hydration in perfluorinated polyelectrolyte membranes such as Nafion is essential to maintaining good ion conductivity and managing permeation, especially in vapor-fed devices where water content depends on relative humidity in a gas stream. Extensive studies in the literature have shown that Nafion hydration in water vapor is controlled by its interfacial transport resistance. Nafion forms a fluorine-rich layer at the polymer-gas interface, and it has been proposed that this layer blocks water transport due to its hydrophobicity. To develop a molecular-level description of the physics underlying transport resistance in this system, we have performed a computational reaction-diffusion kinetics study of water evaporation from Nafion. Two distinct models are examined, one mimicking the blocking function proposed in the literature, the other assuming there is no blocking, instead treating water evaporation as a dynamic balance between uptake from the gas and desorption from the polymer surface. Simulation results are compared to time-dependent infrared data over a range of 100%-0% relative humidity from the literature. Only the dynamic model successfully reproduces experimental observations. This indicates that the physical nature of interfacial transport resistance is not slow diffusion across an interfacial layer, rather it is due to the competition between dehydration and rehydration. The simulation data provide details on the accompanying

1

water distributions throughout the membrane and on interfacial kinetics, showing that they are characterized by strong fluctuations.

Keywords: Nafion, dehydration, simulations, hydrophobic, diffusion, water, vapor

I.   INTRODUCTION

Perfluorosulfonic polyelectrolyte membranes (PFSA) such as Nafion are key components in artificial photosynthesis systems, where transport of ions and blocking of product crossover are central to function.[1] When used as membrane separators in vapor-fed systems such as gas diffusion electrodes (GDE) and membrane electrode assemblies (MEA) for solar fuels systems,[2] they are often installed with one side in contact with vapor and the other with liquid electrolyte to stabilize the extent of hydration of the membrane in use. They are also used as ionomer layers in GDE and MEA architectures that support an active electrocatalyst for CO_2 reduction, in configurations where they are fed with water. Stable hydration is important because ion conductivity is sensitively dependent on water content in the membrane, and drying reduces catalytic efficiency by increasing the resistance of the system.[3] The availability of water at the catalytic center also influences the catalytic reactions themselves.[4] Predictive models that incorporate detailed, time-dependent catalytic chemistry as well as the molecular-level processes influencing the local concentration of water at the membrane-catalyst interface are central to understanding how vapor-fed artificial photosynthesis systems function during the diurnal sunlight cycle.

Quantification of water in vapor-fed architectures requires knowledge of how water moves into, out of and through the membrane under all conditions. Although the solution-

2

diffusion model is very successful at explaining steady state behavior,[5] there is no similar theory for the time-dependent permeability of membranes, and there are few experimental data for permeability far from steady state. To develop an understanding of non-steady-state processes in general, we have performed experimental and reaction-diffusion modeling studies of gas permeation through rubbery[6] and glassy polymers,[7] as well as aqueous methanol permeation through Nafion,[8, 9] to build basic simulation frameworks that are applicable to diverse systems. We can use these frameworks together with a detailed molecular mechanism that has been developed for pure water evaporation[10] as building blocks to model time-dependent water permeation into and water evaporation from polyelectrolyte membranes used in GDEs and MEAs. The missing mechanistic elements for a molecular-level model of the catalyst-membrane environment in vapor-fed systems are gas-phase water uptake and dehydration. In this work, we focus on the dehydration mechanism using data for Nafion, which is representative of PFSA membranes and a relatively simple evaporation system to model because drying-induced structural changes in the membrane over periods of many minutes do not influence diffusion significantly.[11, 12]

   To construct a model, we focus on what has been learned about the internal and interfacial structures of hydrated PFSAs including Nafion. Their internal structure changes as their extent of hydration changes,[13] leading to development of an internally phase-segregated structure.[14, 15] Hydrophilic channels are formed that can accommodate large molar fractions of water, typically expressed as the number of water molecules per sulfonic acid group, or λ, surrounded by fluorocarbon-rich hydrophobic regions. These channels are responsible for transport of ions across the membrane, and their characteristics directly control its proton conductivity.[16] The values of λ obtained using vapor as the source of water range up to about 15

3

at 100% relative humidity (RH) and an ambient temperature of about 25 °C.[14, 17] The structure of water in these channels, and interactions between water and the hydrophilic sulfonic acid groups within the channels have been examined in bulk films. Nuclear magnetic resonance spectra obtained with a systematic variation of the degree of hydration have shown that diffusion coefficients D increase with increasing hydration, with an activation energy for diffusion decreasing from 42 kJ/mole to 20 kJ/mole as λ increased from 2 to 15.[18] D increases from 0.1 to 0.5 x 10^{-10} m^2/s for $\lambda = 2$-8, then jumps to 2 x 10^{-10} m^2/s for $\lambda = 9$-16. The waters in the sulfonated channels have been identified to be in several states. Water is tightly held by the sulfonic acid site when $\lambda = 1$-2, bound in a solvation shell for $\lambda = 3$-6, and loosely held, or mobile beyond $\lambda = 6$. This is consistent with changes observed during thermogravimetric-infrared analyses during desorption,[17, 19] and with computational studies showing that minimally hydrated sulfonic acid groups inside the channels are very stable.[20] It has been shown that there is heterogeneity to the local value of λ for an average degree of hydration.[21] A synchrotron infrared (IR) study of hydration kinetics as a function of RH[22] showed that at 60 °C there is a residual amount of water at 0% RH, with $\lambda = 1$. $\lambda = 3$ is the threshold for proton mobility, with no further changes in the water spectra as the water concentration increases in the membrane. At room temperature, the residual water is about $\lambda = 2$.[14]

The structure of the PFSA-gas interface very different from that of the bulk, and varies with RH. The membranes develop a hydrophobic, fluorine-rich skin layer in contact with humidified air.[13, 23] Grazing incidence small angle x-ray scattering and atomic force microscopy measurements on Nafion[24] show the layer thickness to be in the range of a few nm. Contact angle measurements showed that the membrane surface is hydrophobic in contact with vapor to 97% RH, and its surface energy does not change during drying in ambient atmosphere.[25] The

4

membrane's surface morphology has been studied as a function of hydration, identifying ion-conducting regions as well as hydrophobic domains and showing a connection between ion conductivity and water content.[26, 27] That there are more hydrophilic regions than ion conducting channels at the surface suggests that water channel connectivity to it is low.[28] Although the surface of the membrane is hydrophobic, water is not absent. Sum-frequency generation spectroscopy of surface water on Nafion as a function of RH revealed that water is adsorbed on both the hydrophilic sulfonate groups and on the hydrophobic surface regions in both free and ice-like forms.[29] Molecular dynamics calculations on interfacial structure and transport show that while there is no change in mass transport (treated as vehicular diffusion) at the interface, there is a decrease in fully hydrated hydronium ions, which is due to a reduced probability of forming Eigen ions, and that the hydronium ions have a preferred orientation at the surface.[30]

The interfacial skin layer has been proposed to be the origin of interfacial water transport resistance. The dominant hypothesis is that the hydrophobic layer controls interfacial water activity relative to water activity in the vapor phase, and thereby acts as a barrier to mass transport of water in and out of the membrane. This barrier property establishes the degree of hydration of the membrane at a particular RH and confers a relatively flat water distribution throughout the membrane.[12, 31, 32] A molecular dynamics study[33] points to a physical mechanism: the hydrophobic layer's mass transfer resistance is attributable to inhibition of diffusion by the semi-crystalline nature of the surface layer.

To summarize, the literature shows that the water content of PFSA membranes at any particular RH is governed by the external and interior water activities intrinsic to that humidity, and the characteristic time to reach that water content is controlled by the hydrophobic membrane-vapor interface's mass transport resistance. What is missing is a molecular-level

5

description of how the internal and external activities are connected, *i.e.* how the membrane's degree of hydration as RH changes is connected to the fluxes of water across the interface, and how these fluxes are coupled to the internal gradient-driven diffusion of water diffusion given that the gradient is small. Such an understanding is essential to be able to model the details of the interfacial catalytic chemistry when it is coupled to membrane drying and hydration of a solar fuels system.

To make progress toward a useful description of interfacial hydration and transport, we have made a computational study of the simple case of dehydration of Nafion from 100% RH to 0% RH that compares the predictions to real-time experimental attenuated total reflection - Fourier transform infrared (ATR-FTIR) differential desorption data from the literature.[34] We start with a model that represents the interfacial transport resistance using the accepted *blocking* characteristics of the Nafion-vapor interface, and show that it cannot reproduce real-time experimental observations. An alternative model that represents the interfacial transport resistance as a kinetic process involving a rapidly maintained *dynamic* balance between water vapor absorption and desorption successfully describes the experimental measurements. Under this model, dehydration and rehydration are in competition at any given RH, resulting in a specific water content at the membrane interface and in its bulk that depends sensitively on both internal and external conditions. While specific data for Nafion have been used to construct both models for comparison to experiment, the dynamic model framework is likely to be applicable to similar PFSAs, and hydrophobic-hydrophilic phase-segregated membranes in general.

II.   MODEL CONSTRUCTION

II.a. Representation of the evaporation process. The experimental study examined in this work

is of real-time ATR-FTIR data measuring water content within 0.5-1 μm of a Nafion - ZnSe

ATR crystal interface during drying at specified RH.[34] To model this experiment, the simulation

framework uses a 1-dimensional array of diffusion-coupled polymer compartments with two

opposing interfaces: one side of the membrane in contact with the crystal, and the other in

contact with water vapor. The framework's description of the water vapor-membrane

interactions is of central importance in this work, and two very different descriptions are

considered as illustrated in **Figure 1**. While the descriptions differ in their treatment of

interfacial processes, they are identical in their treatment of bulk processes which involve both

immobile water attached to sulfonate groups, and mobile water that can diffuse freely.
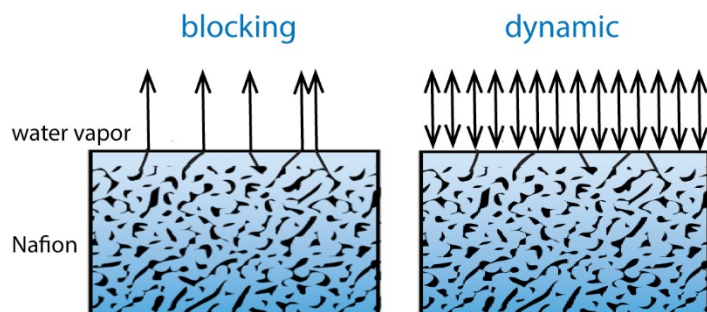

Figure 1. Schematic of the interfacial processes involved in the *blocking* and *dynamic* models for interfacial transport resistance during water evaporation from Nafion. Black represents water-filled regions, whereas blue represents hydrophobic regions. The *blocking* model assumes that water can evaporate only from a small (sulfonated) fraction of the membrane surface. The *dynamic* model assumes that water evaporation can occur from anywhere on the membrane surface, whether fluorine-rich or sulfonated.

Blocking model. This model was considered first because it is a direct representation of findings

in the literature in a reaction-diffusion form. Because the rate of water desorption is controlled by

the interfacial mass transport resistance rather than bulk mass transport resistance,[12] drying is

determined by the net diffusive outflux of water across the perfluorinated hydrophobic skin layer

as proposed in the literature.[26, 35, 36] As illustrated in **Figure 1**, water movement into and out of the membrane can take place only from the sulfonated channel openings at the interface. This restriction on the available active surface area necessarily slows the drying rate. Therefore, the *blocking* model represents the effect of the perfluorinated interfacial layer as a reduction in surface area available for evaporation relative to the geometric area. It also considers that there may be a reduced diffusion coefficient for water into the interfacial region relative to water diffusion in the bulk, as suggested by theory.[35] The net diffusive outflux from the active area is described as a reversible adsorption-desorption process where desorption is always at a higher rate due to the higher water activity in the polymer phase.[37] Because we are working at the molecular level, we use concentrations instead of activities, and the evaporation rate is proportional to the gradient between the water concentration inside the membrane (moles/L range) and the outside (10^{-3} moles/L range).

Dynamic model. The *blocking* model has important assumptions about how water moves through the membrane-vapor interface. As will be shown below, it is not successful in reproducing experiments, so an alternative *dynamic* model has been constructed that eliminates the main assumptions in the *blocking* model. First, we treat water adsorption and desorption as not necessarily being reversible, that is, that these steps do not have to both involve the same kinds of molecular environments on the membrane surface. Specifically, we assume that water adsorption and desorption can take place from both hydrophobic and hydrophilic surfaces, *ie* the entire surface is active rather than a small fraction of it. The physical justification for removing the requirement that water can only adsorb and desorb from sulfonated channels in the *dynamic*

8

model is found in the literature on interactions between vapor-phase water and perfluorinated materials. Molecular beam scattering studies of water from perfluoropolyether liquid films show that while most collisions are elastic, about 17% and 29% of the collisions at 66 and 31 kJ/mole incident kinetic energy, respectively, result in trapping with subsequent desorption.[38] Since the probability of trapping-desorption increases as incident kinetic energy decreases, and the kinetic energy of a gas at 303K is $3kT/2 = 3.8$ kJ/mole, trapping-desorption of vapor-phase water on the perfluorinated regions of Nafion could become important at room temperature, leading to long enough lifetimes for adsorbed water to diffuse across the vapor-polymer interface. Evidence that this can occur readily is found in IR observations of reversible, rapid, and nearly complete H_2O exchange with D_2O inside 200 nm thick Nafion films when they are exposed to water vapor.[39] Additionally, an estimate of the partitioning of water between the vapor and perfluoropolyether (PFPE) films gives a value of 0.5 (mol of water/mL of air)/(mol of water/mL of PFPE).[40] Efficient absorption of weakly interacting gases into polymers has been identified in other systems using molecular dynamics: CO_2 into polydimethylsiloxane[6] and CO_2 and N_2 into poly(dimethyl phenylene) oxide.[7] Second, we remove the assumption that the diffusion coefficient for water through the hydrophobic interface is small, because large diffusion coefficients have been measured for water moving through perfluorinated materials.[40-42]

II.b. System Geometry. The framework used in this study for both models is adapted from the one used for modeling permeation of methanol through Nafion.[8] Briefly, the membrane is represented by a 1-D stack of 240 bulk compartments and 1 interface compartment, open at one end to gas and in contact with an ATR-FTIR crystal at the other. The cross sectional area of the

membrane compartments is 0.06 m x 0.01 m, matching the experiments.[34] The total thickness of

the membrane depends on its degree of hydration and varies continuously throughout the

simulations, with a dry membrane thickness of 120 μm estimated from the measured thickness of

the membrane as a function of RH.[34] Calculations of the initial thickness of each compartment

for each RH in the simulations is presented later in this section. The composition of the bulk

compartment adjacent to the ATR-FTIR crystal is used to calculate the infrared signals for

comparison to experiment because the compartment thickness corresponds to the depth probed

by the infrared evanescent wave (0.5-1 μm). All compartments are assumed to have

homogeneous composition at all times. This means that the details of phase segregation and the

water channels are not included in the model, they are represented implicitly by specifying

separately the amounts of sulfonate groups, non-sulfonate polymer and instantaneous water

content in each compartment. The diffusion coefficient D contains information relevant to the

transport of water from one compartment to its neighbors, reflecting the water channel structure.

The flux of water vapor between the gas phase and the membrane does not involve an explicit

gas volume compartment for computational efficiency.

II.c. Reaction-diffusion model construction. The *blocking* and *dynamic* models have the same

structure and composition for the bulk and interfacial polymer compartments, with the same

kinetics in the bulk compartments and differing kinetics in the interfacial compartments.

Concentrations and local volume changes. There are 3 chemical components in each

compartment, whether bulk or interface: sulfonate groups with 2 waters tightly bound to them

10

and therefore immobile at the temperature of the experiments (303K),[19] mobile water, and the non-sulfonate parts of the fluoropolymer.

The water content as a function of RH is not independently quantified in the experimental work, it is reported as an IR signal obtained from the interface between the membrane and the ATR-FTIR crystal during a differential diffusion measurement.[34] To associate the IR signal (reported in arbitrary units) with water concentrations, the absorbance data shown in Figure 5 of Ref [34] have been digitized and scaled assuming that an IR signal of 125 equals $\lambda = 15$ (**Table S1** and **Figure S1** in the Supporting Information). All other IR absorbances are assumed to be linearly proportional to that value. The ATR-FTIR signal is compared to the simulation results by assuming it represents the sum of signals from the two types of waters - those tightly held by sulfonate groups and the mobile waters which are the waters in the solvation shells surrounding the sulfonate groups. The simulations provide information on all water throughout the rest of the membrane, rounding out the picture of dehydration for the full system corresponding to changes at the membrane-crystal interface.

The initial membrane compartment thicknesses are calculated using the amount of dry Nafion in the film at 0% RH, and the amount of water as determined by the value for λ at a specific RH from the IR data, and their densities, which are assumed to be additive. The density of sulfonate groups plus the fluoropolymer are taken to be that of Nafion 117, 2.03 Kg/L,[43] with an equivalent weight of 1.1Kg polymer/mole(sulfonate groups), Nafion 117,[34] and that of water is 55.4 mole/L whether mobile or immobile. The thicknesses and the initial amounts of water and polymer (**Table S1**) in turn determine the initial concentrations, as shown in **Table 1**. As waters move through the membrane, the volume of each compartment is explicitly calculated during the

11

simulations using the instantaneous amounts of polymer and water and their molar densities,

enabling local concentrations and local degree of swelling and deswelling to be tracked

accurately. In our previous ATR-FTIR modeling study the time-dependent permeation of Nafion

was found to be insensitive to the initial thickness assumed for the interfacial layer,[8] so the

assumption of 1 nm of dry polymer was not specifically evaluated in this work.

The concentration of water in the vapor phase is calculated from the reported RH

assuming the experimental temperature of 303K.

Table 1. Initial conditions for evaporation simulations, *blocking* and *dynamic* models, calculated from ATR-FTIR data and densities for H_2O and Nafion.

RH (%)	mobile H_2O (mole/L)	polymer (mole/L)	sulfonate + 2 H_2O (mole/L)	bulk compartment thickness (μm)	interface compartment thickness (nm)
100	16.081	1.237	1.237	0.752	1.50
80	14.227	1.328	1.328	0.700	1.40
56	8.999	1.419	1.419	0.655	1.31
43	6.648	1.510	1.510	0.616	1.23
22	2.737	1.635	1.635	0.569	1.14

The amounts of water and polymer are assumed to have the same initial value in all

compartments, including the interface compartment, at the beginning of each differential RH

change. (Their concentrations will depend on their starting volumes which are determined by

water and polymer densities.) Since all compartments are assumed to be uniform in composition

this assumption builds in a further assumption that the hydrophobic character of the interfacial

layer does not involve an actual increase in the amount of fluoropolymer and decrease in the

amount of sulfonate groups in that compartment, just a compositional inhomogeneity. If there is

net segregation, it is possible that this could lead to differences in water distributions within the

interfacial compartment, however this is neglected because of a lack of experimental data on

near-surface water concentrations to refine the models. There is evidence that the distribution of water within the interfacial compartment could be independent of the specific location of sulfonate regions (beneath the surface) and fluoropolymer rich regions (closer to the surface). Although its overall solubility is low, water dissolved in Teflon tends to form clusters of about 14 waters that are both strongly and weakly H-bonded to each other,[44] providing evidence that the water molecules can find a stable state within the fluoropolymer-rich portion of the interface compartment.

Time-dependence. The experimental evaporation data (**Table S1** and **Figure S1**) were acquired over 5 separate RH steps: 100%-80%, 80%-56%, 56%-43%, 43%-22% and 22%-0%. The Nafion film mounted on the ATR-FTIR crystal was exposed to a gas flow at the specified upper RH in each range for an extended period, allowing the ATR-FTIR signal to stabilize for typically a few 1000's of seconds, then abruptly dropping the RH to a new value. In the simulations this is treated as an instantaneous decrease although in reality the RH will take some time to reach its new value due to water-surface interactions in the apparatus. The impact of assuming an abrupt drop on the simulation results is challenging to assess because the data measure changes far from the vapor-exposed region of the membrane. The exact time of each RH change was not reported. To be able to compare experimental and calculated signals, the experimental data set was divided into segments, with one point defined to be at time = 0 for each segment. The experimental zero is selected so that the time at which the measured signal begins to decrease matches that in the calculations. This shifts, but does not distort the absolute experimental time base.

13

Bulk and interfacial diffusion. The diffusion coefficient D of water between two adjacent bulk

compartments is taken to be a value in the middle of the range of those determined

experimentally by the ATR-FTIR measurements,[11, 34] 5×10^{-11} m^2/s. The sensitivity to this value

was not assessed in this work; the experimental value consistent with the IR data was assumed to

be the most relevant in view of the wide range that has been reported and the variability of

diffusivity with experiment design and sample history.[13] The *dynamic* model assumes that this

value of D is also valid for diffusion between the bulk and interface compartments, as suggested

by measurements of rapid water diffusion through fluorinated matrices.[40-42]. Several variations on

the *blocking* model are examined to evaluate sensitivity to model assumptions, listed in **Table 2**.

In *blocking* model cases A and B, the value for D between the bulk and interface compartments

is reduced to 1×10^{-12} m^2/s to mimic its proposed barrier properties. *Blocking* model cases C and

D incorporate the same value for D as used in the *dynamic* model to evaluate independently the

influence of water channel connectivity to the membrane surface, represented as an effective

surface area for water desorption that is much reduced relative to the geometric area. Case I

Fickian diffusion is assumed for both *blocking* and *dynamic* models: the diffusion rate is

controlled by concentration gradients between adjacent compartments, and their 0.06 m x 0.01 m

contact area. Although there is evidence for polymer structural changes during hydration,

relaxation of these changes is found to be slow relative to the rate of evaporation,[34] and

contributions from Case II or anomalous diffusion are neglected.

Table 2. *Blocking* model cases considered in this study

Case	D, bulk-interface, m^2/s	% of surface active for H$_2$O desorption

14

A	1×10^{-12}	1
B	1×10^{-12}	15
C	5×10^{-11}	1
D	5×10^{-11}	15

Rate coefficients for adsorption and desorption. The primary difference between the *blocking* and the *dynamic* models is in the way that water adsorption and desorption are described. The *blocking* model considers only net water desorption under the assumption that adsorption and desorption are reversible and take place from ion-conducting water channel openings.[35] The literature suggests that interfacial water confined to the sulfonate channels is liquid-like in character.[45] Therefore, in this model we use the mechanism and kinetics determined previously for evaporation of water from a water surface at the molecular level,[10] treating the water aggregates at the water channel openings as very small droplets.[29, 46] Briefly, in the previous study kinetics simulations of evaporation from pure water droplets as a function of RH and temperature have shown that water desorption from water is a combination of first order (Hertz-Knudsen[47]) and third order net desorption processes.[10, 48] The Hertz-Knudsen model assumes that adsorption and desorption are microscopically reversible processes, and therefore involve simple first order liquid-gas phase transitions, and the third order step involves a sequence of water-water collisions close together in time to break hydrogen bonds. The Hertz-Knudsen expression is for a net flux, *i.e.* the difference between water adsorption and desorption rates at a particular temperature and RH, thereby incorporating adsorption indirectly. The rate coefficients for pure water evaporation determined in the previous study[10] have been validated using experimental

15

data and shown to be predictive, and we assume they are applicable to the Nafion drying model at the experimental temperature of 303K.

In the present study, the *blocking* model is only evaluated for one RH range, 100%-80%. This is because it quickly became clear through the simulations that it does not successfully describe membrane drying and further calculations would not be informative. Base values for the 1st and 3rd order water desorption steps at 80% RH used for *blocking* models A-D are presented in **Table 3**. The added assumption in the *blocking* model is that only a fraction of the geometric surface area is active, and this fraction is used to scale the base desorption coefficients by 0.01 (cases A and C) and 0.15 (cases B and D), **Table 2**.

The *dynamic* model does not consider adsorption and desorption to be reversible steps, and therefore includes them as separate processes. This relaxes the constraint inherent in the Hertz-Knudsen description that adsorption and desorption must take place from the same kinds of surface sites, for example from water at sulfonate channel openings. The most general assumption is that adsorption rate is proportional to the water vapor flux to the entire 6×10^{-4} m^2 Nafion surface at 303K. To avoid explicitly modeling gaseous water, which is computationally prohibitively expensive using stochastic methods, the adsorption step is represented as a reaction having zeroth order kinetics. The value for the adsorption rates at each RH (shown in **Table 3**) is obtained from the gas kinetic flux. Gas-solid collisions do not generally result in 100% efficiency for sticking, i.e. residence times on the surface long enough for absorption to occur in the case of polymers. Sticking with 100% efficiency is represented as a sticking coefficient of 1. Here, we assume a sticking coefficient of 0.5 at each flux, i.e. 50% of the collisions at the polymer-vapor interface result in water permeation into the membrane. This value is a rough order-of-magnitude

16

estimate, but is reasonable given the very weak interactions between water and perfluorinated materials. Large sticking coefficients have been calculated using molecular dynamics for other weakly interacting gas-polymer systems CO_2 into polydimethylsiloxane (0.3)[6] and poly(dimethyl phenylene oxide) (minimum of 0.13).[7] Further, water is observed to partition into the perfluoroether-on-sulfuric acid system with an efficiency of 50%.[40] Because desorption and adsorption are not assumed to be reversible, the desorption rate coefficient is treated as an unknown. To estimate its value, it is incorporated in the model as a fitting parameter to reproduce the 100% RH to 80% RH decrease data as will be described in the next section. This is the only fitting parameter used in this study. The fitting process can be considered to be a measurement of the rate coefficient. Its value is held constant to simulate the other RH conditions.

Table 3. Interfacial rate coefficients

Final RH (RH decrease range)	*Blocking* model, base H_2O desorption rate coefficients (scaled by 0.01 or 0.15)		*Dynamic* model, H_2O adsorption flux
	1st order (s^{-1})	3rd order ($L^2/mole^2$-s)	(mole/L-s)
80% (100%-80%)	662	1.42 x 10^7	7.34 x 10^7
56% (80%-56%)	--	--	5.14 x 10^7
43% (56%-43%)	--	--	3.95 x 10^7
22% (43%-22%)	--	--	2.02 x 10^7
0% (22%-0%)	--	--	0

II.d. Simulation methods

The simulations provide complete spatially-resolved concentration vs time data in the membrane for comparison to experiment. Calculations of both the *blocking* and the *dynamic* models are performed using the open access software package Kinetiscope,[49] which uses a stochastic

algorithm originally developed for homogeneous systems[50, 51] that has been extended to full

reaction-diffusion schemes to calculate the complete time history of the system.[52] The models are

constructed using the system geometries, reaction-diffusion steps, initial conditions such as

thickness of the swollen membrane, and densities and concentrations as inputs. Use of

physically-based elementary rate coefficients and materials properties ensures that the physics

and chemistry of the system are fully represented. Because the stochastic method provides a

rigorous solution to Markov systems and generates an absolute time base, the calculations are

predictive and can be compared directly to experimental data. The computational method is

particularly useful for inductive mechanism discovery,[53] when parts of the reaction mechanism

are not well-understood and are identified through construction of scenarios and increasingly

complex schemes. It is also well-suited to multiscale modeling, where broad ranges of time and

length scales are simulated in a single calculation.[54] A particular advantage of stochastic methods

over the continuum methods that are more commonly used to model membrane transport is the

ability to capture instantaneous volume (and local concentration) changes as well as fluctuations

in the local environment in both the membrane bulk and at the interfaces.

The stochastic kinetics simulation is a type of kinetic Monte Carlo, and has the

characteristic that simulations of fast, coupled reversible processes are inefficient. Some of the

calculations reported here were affected by this and were not carried longer than about 500 -

600s in simulation time, which took over a week in physical time on a fast microprocessor. The

criterion for ending a simulation was if the water content in the Nafion film at the ATR-FTIR

crystal interface was no longer decreasing significantly, as was observed experimentally.[34]

Because no differential equation integration is involved in these calculations, it is

possible to structure the reaction scheme to include marker species that are not reactants or

18

products, but serve as counters for the number of times a particular reaction step occurs in a specified location. This is a powerful tool to extract additional insights from the simulation results. In the present study, markers are used in the interface compartment to track water adsorption and desorption events. The first order desorption step for mobile water at the interface for both models is

$$\text{water} \xrightarrow{} gas \tag{1}$$

The third order desorption step in the *blocking* model is

$$3 \text{ water} \xrightarrow{} 2 \text{ water} + gas \tag{2}$$

and adsorption in the *dynamic* model is written

$$\text{polymer} \xrightarrow{} \text{water} + \text{polymer} + adsorbed \tag{3}$$

where *gas* and *adsorbed* are marker species that have zero partial volume and therefore do not contribute to instantaneous thickness calculations.

III. RESULTS AND DISCUSSION

III.a. Comparison of the blocking and dynamic models at 100%-80% RH

The mobile and sulfonate water concentrations calculated in these simulations are converted to an IR signal for comparison to experimental measurements,[34] as shown in **Figure 2**. Five sets of simulations have been performed: the *blocking* model, cases A-D, and the *dynamic* model. As noted above, the rate coefficient for desorption in the *dynamic* model is unknown, and had to be treated as a fitting parameter for the 100%-80% RH data set. It is the only unknown. The best value for the desorption rate coefficient is estimated to be $5.4 \pm 0.2 \times 10^6 \text{ sec}^{-1}$. The error in this case reflects only the sensitivity of the fit. Other sources of error include the exact

19

correspondence of the IR signal to water concentration, the actual time profile for the decrease in

RH during the measurements, and the assumption of a sticking probability of 0.5. It is not

possible to assess the magnitudes of these sources of error without further experimental work. A

test of the validity of this value is whether it can successfully predict IR data for the other RH

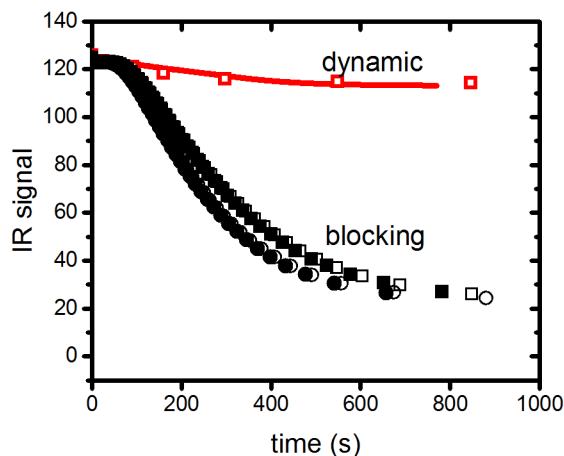ranges, which will be discussed in the next section.

Figure 2. Experimental (red squares) infrared signal detected at the ZnSe-Nafion interface for an RH decrease from 100 to 80%, compared to predictions from the *dynamic* model (red line) and the *blocking* model Case A (black open squares), Case C (black closed squares), which have 1% of the surface area active for desorption, and Case B (black open circles), Case D (black closed circles), which have 1% of the surface area active for desorption.

Although the experimental data show a minimal reduction in the IR signal, and therefore

minimal drying under these conditions, all 4 *blocking* cases predict nearly complete evaporation

of mobile waters at 80% RH, with the 2 remaining waters being strongly bound to the sulfonate

groups. *Blocking* model cases A-B and C-D predict very similar IR signals for the 1% and 15%

effective surface areas, indicating that reduction of *D* by a factor of 50 has a minimal impact on

20

the kinetics. This is counterintuitive, and at odds with the proposal that drying rate of Nafion is

controlled by the presence of a hydrophobic layer that inhibits interactions with water. In order to

understand this result, we can examine additional details about the desorption process for both

models. **Figure 3a** shows that the concentration of water in the interface compartment for

blocking model Case A is extremely low, while the *dynamic* model predicts it to be high. This is

a consequence of the kinetics of water evaporation from very small droplets (*blocking*) rather

than the full membrane surface (*dynamic*).[10] **Figure 3b** shows the corresponding evaporation rate

for the two models, calculated from the derivative of the time-dependent count of *gas* markers

for both models. The data show that despite the large differences in interfacial concentrations, the

evaporation rates have a similar order of magnitude. The *blocking* model predicts a finite

evaporation rate, as is expected from its representation of water evaporation as always faster than

water absorption, while the *dynamic* model fluctuates between positive and negative values for

the evaporation rate once the rate is near zero after the first 50-100s. This means that under the

dynamic model, net evaporation and net absorption both occur, leading to a relatively low overall

extent of drying. The corresponding maps of mobile water concentration as a function of time

through the full thickness of the Nafion film are shown in **Figures 3c** and **3d**. The water

distribution decreases smoothly as a function of time under the *blocking* model, and has a steep

gradient. The prediction that drying is fast although the water concentration at the interface is

low points to this gradient as being kinetically controlling, i.e. under the *blocking* model

evaporation is controlled by bulk water transport. The *dynamic* model shows very different

behavior, with slow fluctuations in water concentration especially near the Nafion-water vapor

interface. The relatively small water gradients and large water concentration at the interface

indicate that the near-zero net evaporation rate is due to interfacial processes being rate controlling. The spatial distribution of water is in agreement with previous proposals in the literature, however the physical origin of this distribution and how it is connected to the interfacial transport resistance is significantly different.[12, 31, 32]
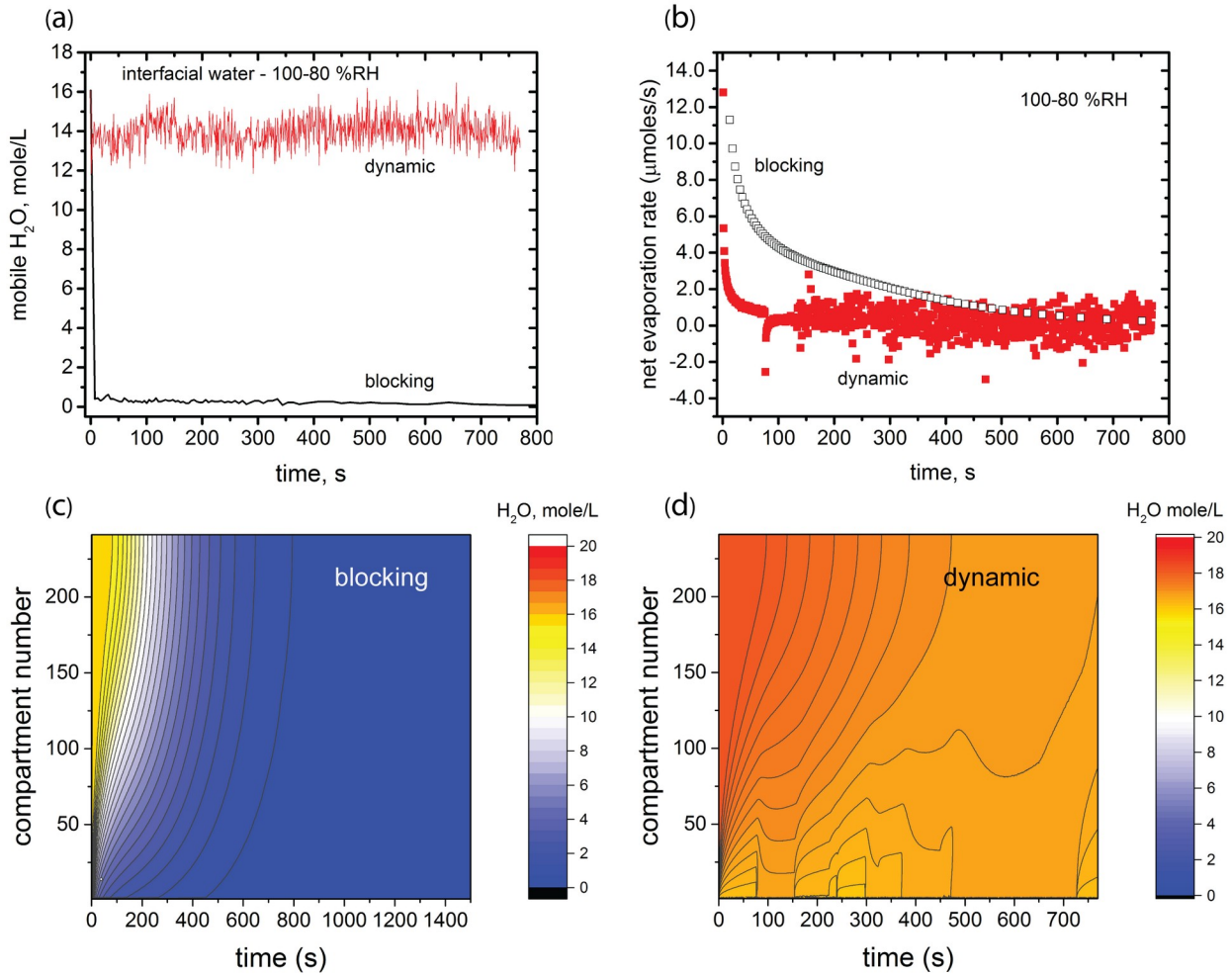

Figure 3. Comparison of simulation results for the case of RH decreasing from 100% to 80%. The *blocking* model is Case A. The maps in the figure are oriented so that compartment 1 is the Nafion-water vapor interface and compartment 241 is the Nafion-ATR-FTIR crystal interface. (a) concentration of mobile water at the vapor-Nafion interface for both models. (b) Water evaporation rate from the vapor-Nafion interface for both models. (c) Map of mobile water concentration as a function of position and time for *blocking* model Case A. (d) Map of mobile water concentration as a function of position and time for the *dynamic* model.

It is notable that the value for D in bulk Nafion used here, 5 x 10^{-11} m^2/s, is in the same range as that measured for water diffusion through fluorinated materials. Water diffuses readily through Teflon, with D estimated to be 2-7 x 10^{-11} m^2/s.[41, 42] Measurements of diffusion of water through perfluoropolyether liquid films on sulfuric acid gave a coefficient of about 6 x 10^{-10} m^2/s.[40] The measured diffusion coefficients suggest that once water crosses the perfluorinated surface and moves into the membrane, it can move just as freely through a fluoropolymer as has been measured for the water channels of Nafion, although its solubility is low so tends to accumulate in the hydrophilic regions around the sulfonate groups.[13]

The simulations comparing these two models to experimental observations provide evidence that the commonly invoked picture that a hydrophobic skin confers a significant interfacial transport resistance due to being a barrier that controls the evaporation rate of water from Nafion is not likely to be correct. Hydrophobicity is assessed by contact angle measurements using liquid water, however liquid-polymer wetting is not the same as gas-solid collisions. The hydrophobic layer facilitates dynamic exchange of water molecules with the surrounding vapor because it interacts so weakly with them, and the continual interplay between adsorption and desorption is the primary physics underlying interfacial transport resistance. This finding is consistent with an analytical vaporization exchange model, proposed in conjunction with a detailed experimental study, that considers water uptake and evaporation to be balanced at steady state, analogous to the electrochemical exchange current density.[55] The present work shows this picture to apply far from steady state as well.

The value for the desorption rate coefficient estimated using the *dynamic* model, 5.4 ± 0.2 x 10^6 sec^{-1}, can be used to calculate an apparent activation energy for water desorption from the Nafion surface, assuming that the only waters that have appreciable concentrations are bound to

23

sulfonate groups at the interface. Assuming a transition state theory Arrhenius A factor of kT/h, 6.31×10^{12} s^{-1} and dividing the desorption rate coefficient by this value, we predict an activation energy for desorption of a water molecule from the Nafion surface of 35.1 kJ/mole. The activation energy for vaporization of water from water has been measured to be 43.8 kJ/mole,[56] while that for fluoropolymer has not been measured, but is likely to be very low, of the order of a van der Waals binding energy.[57] If the estimated activation energy reflects only the endothermicity of removing a water, with no extra barriers, it can also compared to theoretical binding energies for waters to triflic acid, about 50.2 kJ/mole,[58] and to the sulfonic acid group in lithiated Nafion, about 80 kJ/mole.[59] These comparisons raise the possibility that the fitted water desorption rate coefficient in the present simulations reflects desorption from a range of strongly and weakly bound sites (ie sulfonated groups, water droplets and fluoropolymer, as has been observed spectroscopically[29]). Experimental studies would be valuable to evaluate whether this possibility is correct.

III.b. Comparison of the dynamic model to experimental data from 100% RH to 0% RH

The *dynamic* model is used to predict the IR measurements for the other RH ranges with no further changes to the kinetic parameters except the incident water vapor flux and initial
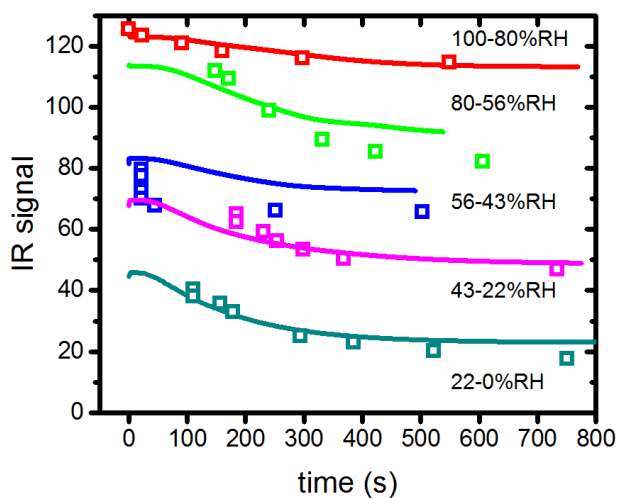
24

Figure 4. Experimental (symbols) and predicted (solid lines) infrared signals measured at the membrane-ATR-FTIR crystal interface as a function of RH.

amount of water appropriate to the starting RH as determined experimentally. As shown in

Figure 4, the simulations are in excellent agreement with the data for the 43-22% RH and 22-0%

RH measurements. The agreement is less good at 80-56% and 56-43% RH, where the calculated

signals are about 10% higher than observed. That there is a deviation only for these two data sets

raises the possibility that the experimental RH was a bit lower than the stated value of 56%.

Overall, agreement with experiment supports that the *dynamic* model is a valid description of the

evaporation process.

The simulations provide detailed time-resolved information about all parts of the water

Nafion system, including spatial distributions for mobile water and instantaneous local partial

volume changes (**Figure S2**) as the membrane deswells. Water concentration maps are shown in

Figure 3d for the 100%-80% RH simulations, and **Figure 5** for the 80%-0% RH series. They are

remarkable in that they show water concentration fluctuations over long time scales. This was a

most unexpected finding. Additional simulations with different random number sequences and

sets of initial conditions have been performed to evaluate whether the fluctuations are an artifact

of the stochastic simulation itself,[49-51] and have ruled out this possibility. Concentration and local

partial volume fluctuations are always observed but their exact timing and magnitude vary with

the initial random number used to seed the event selection cycles in the code, consistent with

their being sporadic in nature. The fluctuations are most pronounced near the vapor-membrane

interface, but can at times penetrate to about half way through the membrane. They become less

pronounced as RH is reduced.

25

The amounts of water in each compartment in **Figures 3d** and **5** are used to calculate the total mobile plus sulfonate-bound water in the film as a function of time and RH conditions, as presented in **Figure 6** with additional detail for the 100%-80% RH range shown in **Figure S3**. It can be seen that the fluctuations are present in the total water amounts as well, especially down to 43% RH. Previous studies of water distributions within a Nafion membrane have not reported time-dependent data that could potentially be compared to these predictions over the entire RH range. There is one report of noisy oscillations of total water in Nafion during hydration at 95-100% RH using a highly sensitive balance.[12] The authors proposed that these could be due to evaporation and condensation of droplets on the sample or sample support, although the water vapor is not supersaturated. Experimental and computational studies of pure water aerosol held at constant RH show that mass changes in water droplets are monotonic in nature, however, without evidence for alternating evaporation and condensation.[10, 60] The simulations reported here suggest that the fluctuations could also have originated at least in part from changes in the amount of water inside the Nafion membrane. New experimental studies to test the model predictions would be very valuable.
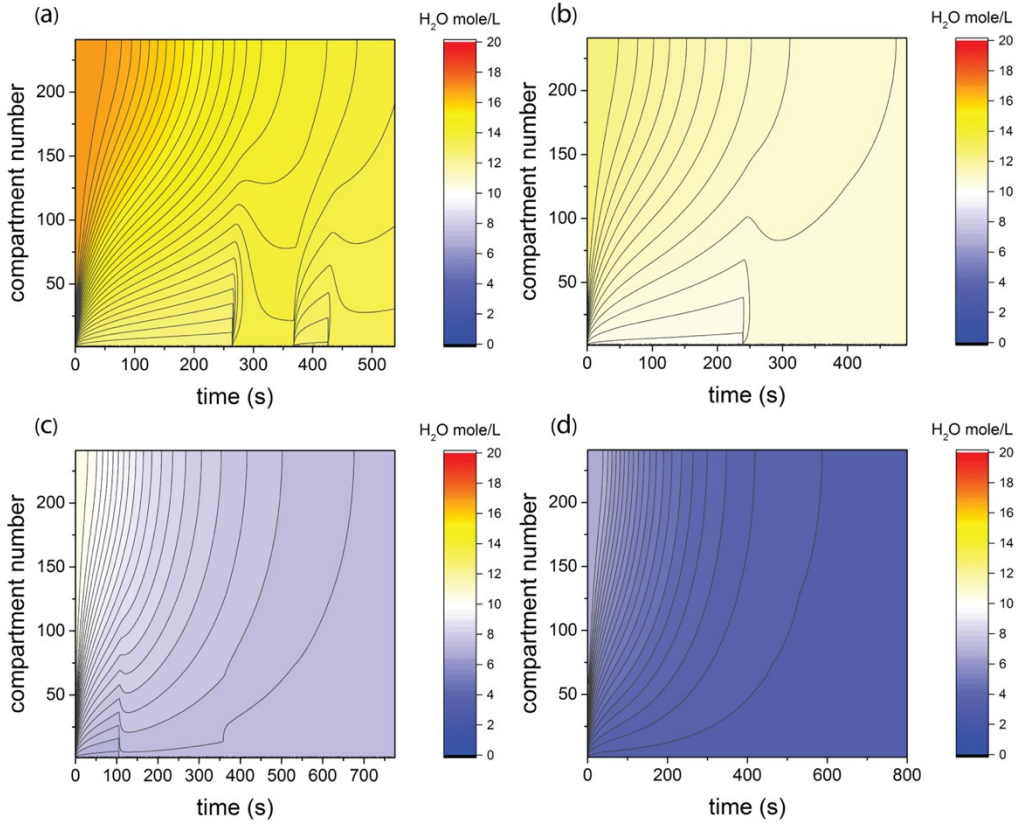
26

Figure 5. Maps of mobile water concentration in Nafion as a function of position and time. The maps are oriented so that compartment 1 is the Nafion-water vapor interface and compartment 241 is the Nafion-ATR-FTIR crystal interface.(a) 80-56% RH; (b) 56-43% RH; (c) 43-22% RH; (d) 22-0% RH.
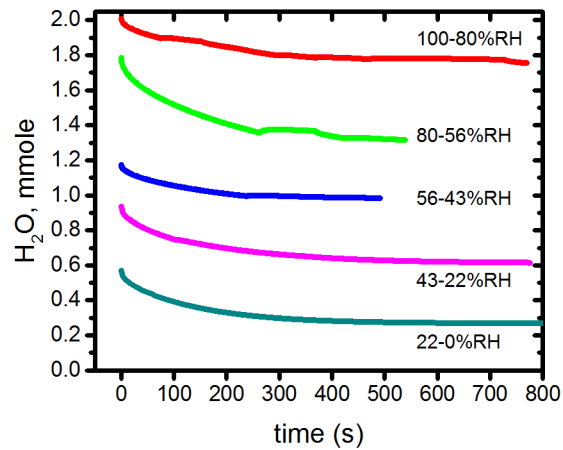

Figure 6. Total water amounts (mobile + bound to sulfonate groups) as a function of time in Nafion.

27

Water concentration fluctuations are also observed in the membrane interfacial compartment, as illustrated in **Figure 3a**, and shown for all RH in **Figure 7a**, together with the interfacial evaporation rates calculated from the difference between the derivative of *gas* vs time (desorption) and *adsorbed* vs time (adsorption) in **Figures 7b** and **S4**. Over the range of 100%-22% initial RH, the rate of water evaporation is high at first, rapidly decaying to a low value with strongly fluctuating levels of adsorption (negative rate) and desorption (positive rate). The 22%-0% RH case shows only desorption because the RH at the vapor-Nafion interfaces is assumed to be maintained at 0% and adsorption of water does not occur. The net evaporation rates show a very similar time dependence despite the wide range in water vapor pressure. The RH-dependence of the interfacial water concentration of water is strong as shown in **Figure 7a**, reflecting the balance between the rate of water evaporation and of its resupply from adsorption and possibly internal diffusion driven by the local concentration fluctuations (**Figures 3d** and **5**).

The data in **Figures 5** and **7** show that the local hydration of the membrane is extremely responsive to RH and will fluctuate around average values especially if RH is closer to 100%. The water content undergoes both rapid fluctuations at the interface, and slow fluctuations in the bulk. These findings indicate that the interfacial transport resistance in Nafion is due to the competition between desorption and rehydration, and that the weak interactions between water and the fluorine-rich regions at its vapor interface facilitate this process. According to the *dynamic* model, if active catalysts are supported on the membrane, the catalytic environment may also fluctuate, potentially influencing selectivity and efficiency for reaction steps involving water or species dissolved in it. For example, it is known from *in situ* studies that water

28

influences the reactivity of CO_2 on Cu and Ag, the most widely studied catalysts for CO_2 reduction.[61, 62] Although the present work addresses only evaporation, the mechanism can be used for hydration if suitable polymer relaxation kinetics are also included.
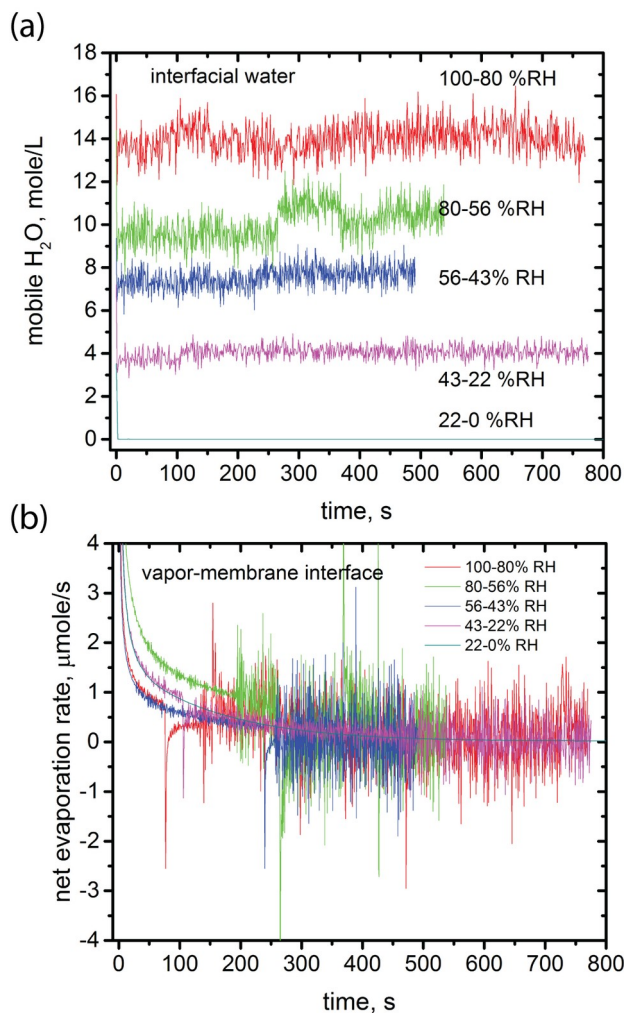

Figure 7. Interfacial kinetics, *dynamic* model. (a) Concentration of mobile water in the interfacial compartment, moles/L, for each RH range. (b) Net water evaporation rate (desorption rate – adsorption rate) from the interfacial compartment into vapor, µmoles/s, for each RH range. The rate can be positive or negative.

III.c. Dynamic interactions between membranes and gases

29

The simulation results presented here show that the interaction between a polymer membrane and its surrounding gas is not always describable as a one-way process dependent only on the solute's activity in the gas and condensed phases, as embodied in the solution-diffusion model. This is consistent with a previous report of exposure of thin Nafion films to alternating atmospheres of D_2O and H_2O up to RH of about 70% that showed rapid and complete replacement of one for the other inside the membrane, as observed by infrared spectroscopy.[39] The authors did not remark on this observation; however, this could only occur if water vapor is continually moving in and out of the polymer at steady state. Strong fluctuations in permeant concentrations have also been observed in our previous studies of the aqueous methanol - Nafion system when simulations are carried through to full system equilibration and involve both in- and out-diffusion of the permeant at the interfaces.[9]

The present results also help explain a finding that puzzled us in our previous studies of permeation of rubbery and glassy polymers by inert gases.[6, 7] In those investigations, we found that time-dependent permeabilities over a large pressure range could only be accurately modeled if the membrane's internal concentration of the permeant as determined by Henry's Law tracked the external pressure rise in the apparatus exactly, leading to net uptake. This response is instantaneous for several rubbery polymers, and dependent on the pressure-rise rate for glassy PPO. In the gas-membrane reaction-diffusion modeling we explicitly connected the internal and external concentrations because this was required to agree with experiments and the mechanism for how the internal concentration of permeant could be so well synchronized with external pressure was not clear to us at the time. The present study suggests a possible explanation, however. Gas permeation in our previous work could also be controlled by a dynamic exchange between the gas and polymer phases, with permeants continuously entering and leaving the

30

membrane at both interfaces. This would provide a means for the internal permeant concentrations to adjust rapidly to external conditions.

This study provides nuance to an underlying assumption in the very successful solution-diffusion model for membrane permeation.[5] Under this model, permeability is governed by the permeant's solubility and diffusivity in the bulk membrane, and interfacial properties are not considered to be kinetically controlling. While this model works well at steady state, it does not describe time-dependent processes: the role of the interface can be important and must be directly captured by a model to have a full picture of how the permeation process works. We have shown here and in previous studies that direct reaction-diffusion simulations can be successful in reproducing experimental observations quantitatively, and that they reveal key mechanistic elements involved in time-dependent permeation. Building them into a fundamental theory for time-dependent processes that ties the polymer physics involved in the interfacial processes to that underlying the solution-diffusion model would be very valuable.

IV.   CONCLUSIONS

Multiscale reaction-diffusion simulations are used to model the process of water evaporation from Nafion in the presence of humidified gas, as monitored by ATR-FTIR. The question under study concerns how to describe the interfacial transport resistance in this system at a molecular level in order to be able to merge the evaporation model with time-dependent catalytic models relevant to artificial photosynthesis. The literature indicates that the physical mechanism underlying the interfacial resistance involves the characteristics of a highly fluorinated hydrophobic skin layer at the membrane-vapor interface that inhibits water diffusion from the Nafion bulk to the gas phase. When embodied in a reaction-diffusion *blocking* model,

31

this mechanism does not reproduce the real-time experimental measurements. An alternative

model is proposed that removes the two inhibiting pathways in the *blocking* description: a small

diffusion coefficient in the interfacial region, and adsorption-desorption confined to the openings

of the sulfonated channels in the membrane. The alternative model assumes that the hydrophobic

interfacial layer functions as an element that facilitates water vapor absorption and desorption

over the entire membrane surface, based on literature that shows that interactions between water

molecules and fluorinated materials are weak. Under this mechanism, water uptake and loss are

in *dynamic* balance at a given RH. Comparison of model predictions to the experimental data

show clearly that only the *dynamic* model captures the underlying physical processes involved in

water evaporation from Nafion. This finding indicates that the role played by the hydrophobic

layer is not attributable to its low wettability, as measured using liquid water. Rather, its weak

interactions with water molecules make it functionally porous to water vapor, with transient

adsorbed populations and rapid exchange between the vapor and the membrane bulk. The

dynamic model should also apply to the hydration process, as long as a description of polymer

relaxations, which influence diffusion, are also included.

The experimental data only provide information on water content as a function of time at

the interface with the ATR-FTIR crystal. The agreement between the model predictions and the

measurements allows the simulations to be used to provide a full picture of water concentration

vs time and position in the membrane as it dries and deswells. Notably, the calculations predict

that the balance between adsorption and desorption is dynamic, giving rise to strong fluctuations

in local water content. This is especially pronounced in the part of the membrane located within

10's of μm of the Nafion-vapor interface at RH between 50%-100%. The continual interchange

of permeants between the membrane and its environment may not be unique to Nafion-like

32

systems. Future experimental and theoretical work on how time-dependent interfacial structure and interactions may influence a membrane's permeability will help develop a fully predictive understanding of membrane behavior in electrochemical devices.

ASSOCIATED CONTENT

Supporting information: experimental infrared data; local partial volumes at all RH; total water content; net evaporation rate at all RH; all data in the Figures (Excel).

AUTHOR INFORMATION

ORCID

Marielle Soniat: 0000-0001-6578-8546

Frances A. Houle: 0000-0001-5571-2548

Author Contributions

The project was conceived, work performed and the manuscript written through contributions of both authors. Both authors have given approval to the final version of the manuscript.

ACKNOWLEDGMENT

33

present address: M.S,: LG Energy Solution MI, 1 LG Way, Holland, MI 49423

REFERENCES

1.   Berger, A.; Segalman, R. A.; Newman, J., Material requirements for membrane separators in a water-splitting photoelectrochemical cell. *Energy & Environmental Science* **2014,** *7* (4), 1468-1476.

2.   Higgins, D.; Hahn, C.; Xiang, C. X.; Jaramillo, T. F.; Weber, A. Z., Gas-Diffusion Electrodes for Carbon Dioxide Reduction: A New Paradigm. *Acs Energy Lett* **2019,** *4* (1), 317-324.

3.   Weng, L. C.; Bell, A. T.; Weber, A. Z., A systematic analysis of Cu-based membrane-electrode assemblies for CO(2)reduction through multiphysics simulation. *Energy & Environmental Science* **2020,** *13* (10), 3592-3606.

4.   Todorova, T. K.; Schreiber, M. W.; Fontecave, M., Mechanistic Understanding of CO2 Reduction Reaction (CO2RR) Toward Multicarbon Products by Heterogeneous Copper-Based Catalysts. *Acs Catal* **2020,** *10* (3), 1754-1768.

5.   Wijmans, J. G.; Baker, R. W., The Solution-Diffusion Model - a Review. *J Membrane Sci* **1995,** *107* (1-2), 1-21.

6.   Soniat, M.; Tesfaye, M.; Brooks, D.; Merinov, B.; Goddard, W. A.; Weber, A. Z.; Houle, F. A., Predictive simulation of non-steady-state transport of gases through rubbery polymer membranes. *Polymer* **2018,** *134*, 125-142.

7.   Soniat, M.; Tesfaye, M.; Mafi, A.; Brooks, D. J.; Humphrey, N. D.; Weng, L. C.; Merinov, B.; Goddard, W. A.; Weber, A. Z.; Houle, F. A., Permeation of CO2 and N-2 through glassy poly(dimethyl phenylene) oxide under steady- and presteady-state conditions. *J Polym Sci* **2020,** *58* (9), 1207-1228.

8.   Soniat, M.; Houle, F. A., Swelling and Diffusion during Methanol Sorption into Hydrated Nafion. *J Phys Chem B* **2018,** *122* (34), 8255-8268.

9.   Soniat, M.; Dischinger, S. M.; Weng, L. C.; Beltran, H. M.; Weber, A. Z.; Miller, D. J.; Houle, F. A., Toward predictive permeabilities: Experimental measurements and multiscale simulation of methanol transport in Nafion. *J Polym Sci* **2021,** *59* (7), 594-613.

10.   Houle, F. A.; Miles, R. E. H.; Pollak, C. J.; Reid, J. P., A purely kinetic description of the evaporation of water droplets. *J Chem Phys* **2021,** *154* (5), 054501.

11.   Hallinan, D. T.; De Angelis, M. G.; Baschetti, M. G.; Sarti, G. C.; Elabd, Y. A., Non-Fickian Diffusion of Water in Nafion. *Macromolecules* **2010,** *43* (10), 4667-4678.

12.   Majsztrik, P. W.; Satterfield, M. B.; Bocarsly, A. B.; Benziger, J. B., Water sorption, desorption and transport in Nafion membranes. *J Membrane Sci* **2007,** *301* (1-2), 93-106.

13.   Kusoglu, A.; Weber, A. Z., New Insights into Perfluorinated Sulfonic-Acid Ionomers. *Chem Rev* **2017,** *117* (3), 987-1104.

14.   Hwang, G. S.; Parkinson, D. Y.; Kusoglu, A.; MacDowell, A. A.; Weber, A. Z., Understanding Water Uptake and Transport in Nafion Using X-ray Microtomography. *Acs Macro Letters* **2013,** *2* (4), 288-291.

15.   Katzenberg, A.; Mukherjee, D.; Dudenas, P. J.; Okamoto, Y.; Kusoglu, A.; Modestino, M. A., Dynamic Emergence of Nanostructure and Transport Properties in Perfluorinated Sulfonic Acid Ionomers. *Macromolecules* **2020,** *53* (19), 8519-8528.

35

16.   Kunimatsu, K.; Bae, B.; Miyatake, K.; Uchida, H.; Watanabe, M., ATR-FTIR Study of Water in Nafion Membrane Combined with Proton Conductivity Measurements during Hydration/Dehydration Cycle. *J Phys Chem B* **2011,** *115* (15), 4315-4321.

17.   Laporta, M.; Pegoraro, M.; Zanderighi, L., Perfluorosulfonated membrane (Nafion): FT-IR study of the state of water with increasing humidity. *Physical Chemistry Chemical Physics* **1999,** *1* (19), 4619-4628.

18.   Hammer, R.; Schonhoff, M.; Hansen, M. R., Comprehensive Picture of Water Dynamics in Nafion Membranes at Different Levels of Hydration. *J Phys Chem B* **2019,** *123* (39), 8313-8324.

19.   Shimoaka, T.; Wakai, C.; Sakabe, T.; Yamazaki, S.; Hasegawa, T., Hydration structure of strongly bound water on the sulfonic acid group in a Nafion membrane studied by infrared spectroscopy and quantum chemical calculation. *Phys Chem Chem Phys* **2015,** *17* (14), 8843-9.

20.   Roudgar, A.; Narasimachary, S. P.; Eikerling, M., Hydrated arrays of acidic surface groups as model systems for interfacial structure and mechanisms in PEMs. *J Phys Chem B* **2006,** *110* (41), 20469-77.

21.   Loupe, N.; Abu-Hakmeh, K.; Gao, S. T.; Gonzalez, L.; Ingargiola, M.; Mathiowetz, K.; Cruse, R.; Doan, J.; Schide, A.; Salas, I.; Dimakis, N.; Jang, S. S.; Goddard, W. A.; Smotkin, E. S., Group Vibrational Mode Assignments as a Broadly Applicable Tool for Characterizing Ionomer Membrane Structure as a Function of Degree of Hydration. *Chem Mater* **2020,** *32* (5), 1828-1843.

22.   Dalla Bernardina, S.; Brubach, J. B.; Berrod, Q.; Guillermo, A.; Judeinstein, P.; Roy, P.; Lyonnard, S., Mechanism of Ionization, Hydration, and Intermolecular H-Bonding in Proton Conducting Nanostructured Ionomers. *J Phys Chem C* **2014,** *118* (44), 25468-25479.

23.   Tang, J.; Yuan, W.; Zhang, J.; Li, H.; Zhang, Y., Evidence for a crystallite-rich skin on perfluorosulfonate ionomer membranes. *Rsc Adv* **2013,** *3*, 8947-8952.

24.   Bass, M.; Berman, A.; Singh, A.; Konovalov, O.; Freger, V., Surface Structure of Nafion in Vapor and Liquid. *J Phys Chem B* **2010,** *114* (11), 3784-3790.

25.   Brack, H. P.; Slaski, M.; Gubler, L.; Scherer, G. G.; Alkan, S.; Wokaun, A., Characterisation of Fuel Cell Membranes as a Function of Drying by Means of Contact Angle Measurements. *Fuel Cells* **2004,** *4* (3), 141-146.

26.   O'Dea, J. R.; Economou, N. J.; Buratto, S. K., Surface Morphology of Nafion at Hydrated and Dehydrated Conditions. *Macromolecules* **2013,** *46* (6), 2267-2274.

27.   He, Q.; Kusoglu, A.; Lucas, I. T.; Clark, K.; Weber, A. Z.; Kostecki, R., Correlating humidity-dependent ionically conductive surface area with transport phenomena in proton-exchange membranes. *J Phys Chem B* **2011,** *115* (40), 11650-7.

28.   Bussian, D. A.; O'Dea, J. R.; Metiu, H.; Buratto, S. K., Nanoscale current imaging of the conducting channels in proton exchange membrane fuel cells. *Nano Lett* **2007,** *7* (2), 227-32.

29.   Noguchi, H.; Taneda, K.; Minowa, H.; Naohara, H.; Uosaki, K., Humidity-Dependent Structure of Surface Water on Perfluorosulfonated Ionomer Thin Film Studied by Sum Frequency Generation Spectroscopy. *J Phys Chem C* **2010,** *114* (9), 3958-3961.

30.   Selvan, M. E.; Liu, J.; Keffer, D. J.; Cui, S.; Edwards, B. J.; Steele, W. V., Molecular dynamics study of structure and transport of water and hydronium ions at the membrane/vapor interface of Nafion. *J Phys Chem C* **2008,** *112* (6), 1975-1984.

31.   Satterfield, M. B.; Benziger, J. B., Non-fickian water vapor sorption dynamics by nafion membranes. *J Phys Chem B* **2008,** *112* (12), 3693-3704.

32.   Kientiz, B.; Yamada, H.; Nonoyama, N.; Weber, A. Z., Interfacial Water Transport Effects in Proton-Exchange Membranes. *J Fuel Cell Sci Tech* **2011,** *8* (1), 011013.

33.   Daly, K. B.; Benziger, J. B.; Panagiotopoulos, A. Z.; Debenedetti, P. G., Molecular dynamics simulations of water permeation across Nafion membrane interfaces. *J Phys Chem B* **2014,** *118* (29), 8798-807.

34.   Hallinan, D. T.; Elabd, Y. A., Diffusion of Water in Nafion Using Time-Resolved Fourier Transform Infrared-Attenuated Total Reflectance Spectroscopy. *J Phys Chem B* **2009,** *113* (13), 4257-4266.

35.   He, Q. G.; Kusoglu, A.; Lucas, I. T.; Clark, K.; Weber, A. Z.; Kostecki, R., Correlating Humidity-Dependent Ionically Conductive Surface Area with Transport Phenomena in Proton-Exchange Membranes. *J Phys Chem B* **2011,** *115* (40), 11650-11657.

36.   Hiesgen, R.; Morawietz, T.; Handl, M.; Corasaniti, M.; Friedrich, K. A., Insight into the Structure and Nanoscale Conductivity of Fluorinated Ionomer Membranes. *Journal of the Electrochemical Society* **2014,** *161* (12), F1214-F1223.

37.   Majsztrik, P.; Bocarsly, A.; Benziger, J., Water Permeation through Nafion Membranes: The Role of Water Activity. *J Phys Chem B* **2008,** *112* (51), 16280-16289.

38.   Saecker, M. E.; Nathanson, G. M., Collisions of Protic and Aprotic Gases with a Perfluorinated Liquid. *J Chem Phys* **1994,** *100* (5), 3999-4005.

39.   Davis, E. M.; Stafford, C. M.; Page, K. A., Elucidating Water Transport Mechanisms in Nafion Thin Films. *Acs Macro Letters* **2014,** *3* (10), 1029-1035.

40.   Porter, J. J.; Klassen, J. K.; Nathanson, G. M., Penetration of water vapor through perfluorinated polyether films on concentrated sulfuric acid. *Langmuir* **1996,** *12* (22), 5448-5450.

41.   Hansen, C. M., Water transport and condensation in fluoropolymer films. *Prog Org Coat* **2001,** *42* (3-4), 167-178.

42.   Hansen, C. M.; Just, L., Water transport and condensation in fluoropolymer films (vol 142, pg 167, 2001). *Prog Org Coat* **2002,** *44* (3), 259-259.

43.   Morris, D. R.; Sun, X. D., Water-Sorption and Transport-Properties of Nafion-117-H. *J Appl Polym Sci* **1993,** *50* (8), 1445-1452.

44.   Raichlin, Y.; Marx, S.; Katzir, A., The investigation of water diffusion into teflon copolymer revealed by fiber-optic evanescent wave spectroscopy. *J Phys Chem A* **2007,** *111* (28), 6131-6134.

45.   Mauritz, K. A.; Moore, R. B., State of understanding of Nafion. *Chem Rev* **2004,** *104* (10), 4535-4585.

46.   Takata, H.; Mizuno, N.; Nishikawa, M.; Fukada, S.; Yoshitake, M., Adsorption properties of water vapor on sulfonated perfluoropolymer membranes. *Int J Hydrogen Energ* **2007,** *32* (3), 371-379.

47.   Persad, A. H.; Ward, C. A., Expressions for the Evaporation and Condensation Coefficients in the Hertz-Knudsen Relation. *Chemical Reviews* **2016,** *116* (14), 7727-7767.

48.   Nagata, Y.; Usui, K.; Bonn, M., Molecular Mechanism of Water Evaporation. *Physical Review Letters* **2015,** *115* (23), 236102.

49.   Hinsberg, W. D.; Houle, F. A. Kinetiscope, available at www.hinsberg.net/kinetiscope, accessed March 12, 2021.

37

50.   Bunker, D. L.; Garrett, B.; Kleindienst, T.; Long, G. S., Discrete Simulation Methods in Combustion Kinetics. *Combust Flame* **1974,** *23* (3), 373-379.
51.   Gillespie, D. T., General Method for Numerically Simulating Stochastic Time Evolution of Coupled Chemical-Reactions. *J Comput Phys* **1976,** *22* (4), 403-434.
52.   Hinsberg, W. D.; Houle, F. A. Software Architecture for Stochastic Simulation of Non-Homogeneous Systems. US Patent 5,826,065, 1998.
53.   Bunker, D. L., Simple Kinetic Models from Arrhenius to Computer. *Accounts Chem Res* **1974,** *7* (6), 195-201.
54.   Macnamara, S.; Burrage, K.; Sidje, R. B., Multiscale Modeling of Chemical Kinetics Via the Master Equation. *Multiscale Model Sim* **2008,** *6* (4), 1146-1168.
55.   Monroe, C. W.; Romero, T.; Merida, W.; Eikerling, M., A vaporization-exchange model for water sorption and flux in Nafion. *J Membrane Sci* **2008,** *324* (1-2), 1-6.
56.   Prado, J. R.; Vyazovkin, S., Activation energies of water vaporization from the bulk and from laponite, montmorillonite, and chitosan powders. *Thermochim Acta* **2011,** *524* (1-2), 197-201.
57.   Scatena, L. F.; Brown, M. G.; Richmond, G. L., Water at hydrophobic surfaces: Weak hydrogen bonding and strong orientation effects. *Science* **2001,** *292* (5518), 908-912.
58.   Prakash, M.; Subramanian, V., Ab initio and density functional theory (DFT) studies on triflic acid with water and protonated water clusters. *J Mol Model* **2016,** *22* (12), 293.
59.   Karpenko-Jereb, L.; Rynkowska, E.; Kujawski, W.; Lunghammer, S.; Kujawa, J.; Marais, S.; Fatyeyeva, K.; Chappey, C.; Kelterer, A. M., Ab initio study of cationic polymeric membranes in water and methanol. *Ionics* **2016,** *22* (3), 357-367.
60.   Miles, R. E. H.; Reid, J. P.; Riipinen, I., Comparison of Approaches for Measuring the Mass Accommodation Coefficient for the Condensation of Water and Sensitivities to Uncertainties in Thermophysical Properties. *J Phys Chem A* **2012,** *116* (44), 10810-10825.
61.   Ye, Y. F.; Yang, H.; Qian, J.; Su, H. Y.; Lee, K. J.; Cheng, T.; Xiao, H.; Yano, J.; Goddard, W. A.; Crumlin, E. J., Dramatic differences in carbon dioxide adsorption and initial steps of reduction between silver and copper. *Nature Communications* **2019,** *10*, 1875.
62.   Favaro, M.; Xiao, H.; Cheng, T.; Goddard, W. A.; Yano, J.; Crumlin, E. J., Subsurface oxide plays a critical role in CO2 activation by Cu(111) surfaces to form chemisorbed CO2, the first step in reduction of CO2. *P Natl Acad Sci USA* **2017,** *114* (26), 6706-6711.

TOC Figure